UCRL-18368

University of California

Ernest O. Lawrence Radiation Laboratory

EXPERIMENTAL DETERMINATION OF η_{00} IN $K_L \rightarrow 2\pi^0$ DECAY, USING 4π SOLID ANGLE SHOWER SPARK CHAMBERS
Part I. EXPERIMENTAL METHOD

R. J. Cence, B. D. Jones, V. Z. Peterson, V. J. Stenger, J. Wilson, D. I. Cheng, R. D. Eandi, R. W. Kenney, I. Linscott, W. P. Oliver, S. Parker, and C. Rey

July 15, 1968

Berkeley, California

DISCLAIMER

UCRL-18368

UNIVERSITY OF CALIFORNIA
Lawrence Radiation Laboratory
Berkeley, California

AEC Contract No. W-7405-eng-48

EXPERIMENTAL DETERMINATION OF $|\eta_{00}|$ IN $K_L^0 \to 2\pi^0$ DECAY, USING 4π SOLID ANGLE SHOWER SPARK CHAMBERS

Part I. EXPERIMENTAL METHOD

R. J. Cence, B. D. Jones, V. Z. Peterson, V. J. Stenger, J. Wilson, D. I. Cheng, R. D. Eandi, R. W. Kenney, I. Linscott, W. P. Oliver, S. Parker, and C. Rey

July 15, 1968

Experimental Determination of $|\eta_{00}|$ in $K_L^o \to 2\pi^o$ Decay, Using 4π Solid Angle Shower Spark Chambers*

Part I. Experimental Method

R. J. Cence, B. D. Jones, V. Z. Peterson,
V. J. Stenger, and J. Wilson
Department of Physics and Astronomy
University of Hawaii, Honolulu, Hawaii

D. I. Cheng, R. D. Eandi, R. W. Kenney,
I. Linscott, W. P. Oliver, S. Parker, and C. Rey
Lawrence Radiation Laboratory
University of California, Berkeley, California

Paper submitted
by S. Parker

to the XIV$^{\underline{th}}$ International Conference
on High Energy Physics
Vienna, Aug. 28 - Sept. 5, 1968

July 15, 1968

*This research has been supported in part by the U. S. Atomic Energy Commission Under Contract AT(04-3)-511 at the University of Hawaii and Contract W-7405-eng-48 at the Lawrence Radiation Laboratory, Berkeley.

1. INTRODUCTION

The branching ratio for $K_L^o \rightarrow 2\pi^o$ is measured using approximately mono-energetic K_L^o mesons from $\pi^- p \rightarrow K^o \Lambda^o$ just below $K^o \Sigma^o$ threshold, with the decay gammas detected in a 4π solid angle detector consisting of lead-plate spark chambers and lead and lucite Cerenkov anti-counters. The basic method is to:

(1) make the gamma detection efficiency high enough so that the over-all $K_L^o \rightarrow 2\pi^o$ detection efficiency is not a sensitive function of the chamber parameters and so that most of the background events ($K_L^o \rightarrow 3\pi^o \rightarrow 6$ gammas) are eliminated by the observation of 5 or more gammas,

(2) use kinematical relationships in the K c.m. system to perform the remaining separation,

(3) use spark counting as a redundant check, and,

(4) make all necessary calibrations by two or more independent methods to provide a check on systematic errors.

K_L^o's of known energy are needed so that the gammas can be transformed into the K c.m. system for the analysis of point (2). Since the Bevatron rf structure is not bunched sharply enough to permit a time of flight analysis on directly produced K_L^o's, a secondary pion beam was used. To minimize the inevitable loss of intensity that this entailed, the K_L^o detector was designed to subtend a relatively large solid angle at the liquid hydrogen target and to have a long flight path for K decay. This consequently large decay volume had to be nearly surrounded with a high efficiency (hence thick) gamma detector. The large size of the detector that resulted from this train of reasoning had one immediately important effect (besides scaring us): the showers were generally well separated, permitting the unambiguous identification of most 5, 6, and 7 shower events.

2. THE BEAM

The pion beam was designed for maximum intensity within three limitations:

(1) the maximum momentum was to be just below the $K^0\Sigma^0$ threshold,

(2) the minimum was set to prevent excessive spread of the resultant K^0 momentum distribution (both the $K^0\Lambda^0$ cross section and the K^0 lab momentum fall rapidly as the threshold is approached),

(3) all collimation slits were located so that scattered particles could not reach the liquid hydrogen target.

The primary target in the Bevatron was a 25.4 cm. long, 0.635 cm. wide, 1.27 cm. high aluminum bar with its length chosen to maximize pion production.

Fig. 1 shows the configuration of the major components of the beam. The pions were bent out and momentum analyzed by the Bevatron field. The first quadrupole doublet formed images of the target within the bore of the second doublet which served as a field lens, recombining the accepted momenta at the hydrogen target. The momentum-limiting collimators were placed within the second doublet. The third quadrupole, a triplet, formed a final image at the hydrogen target of the intermediate images within the field lens. The first (5°) bending magnet was inserted primarily to make the beam adaptable for planned future experiments at different pion momenta. The second (40°) bend served to remove degraded, off-momenta particles from the beam. It did not serve as a momentum analyzer since the slits necessary for that would have been visible to the hydrogen target. Finally, the last two bending magnets swept the charged particles into a beam dump. Helium bags were used between the Bevatron thin window and beam monitor counter M_1[1]. A second monitor, M_2, was placed immediately ahead of the hydrogen target, and a third, M_3, after the target and the first sweeping magnet to detect non-interacting particles.

The pion momentum spectrum is shown in Fig. 2. To maintain adequate momentum resolution, the intermediate images in the field lens must be as narrow as possible. This was achieved by using a narrow target and a pion take-off angle at zero degrees to the long axis. Since this angle could not be monitored by observing the width of any intermediate image--those of adjacent momenta always overlap--an indirect method was used. Many forward-going gammas from π^o decay within the target converted, and in turn sent their pairs sharply forward. Gammas produced at other angles were less numerous and usually escape the target without converting. The resultant electron beam was sharply peaked at zero degrees and could be readily monitored with a 90 cm. long, atmospheric pressure, freon-13 Cerenkov counter that was moved into the beam just upstream of the hydrogen target.

To maximize K_L^o production, the liquid hygrogen target was made as long as possible--1.2m--without the K_L^o spectrum being degraded excessively due to pion energy loss. Forward-going gammas, K_L^o's and neutrons entered a gamma filter placed 1.8 m from the downstream end of the target and consisting of four sheets of lead, in succession 2.54, 3.18, 2.54, and 1.90 cm. thick, each one followed by a 0.635 cm. thick sheet of scintillator (L_1 thru L_4) whose output was placed in anti-coincidence with the trigger signal. An interacting pion that sent a K_L^o into the decay volume had the signature $M_1\ M_2\ \overline{M}_3\ \overline{L}_1\ \overline{L}_2\ \overline{L}_3\ \overline{L}_4$. The lead thicknesses were determined empirically and were the minimum possible consistent with a reasonable trigger rate. Additional lead only resulted in small decreases in the trigger rate since the attenuation distance was becoming characteristic of nuclear rather than gamma distances in the region of 10 cm.

Following the filter, the remaining K_L^o's and neutrons passed thru a steel collimator 1.5 m. long, a four-sided anti-coincidence shower counter surrounding the flight path, and then entered a 1 m. cubic decay volume that started 5.5 m. from the end of the hydrogen target.

The K_L^o spectrum is shown in Fig. 3 and was calculated from the pion spectrum of Fig. 2, allowing for ionization energy loss in the liquid hydrogen, and using the known values of $\sigma_{\pi^-p \to K^o\Lambda^o}(E_{\pi^-})$, $\sigma_{total,\pi^-p}(E_{\pi^-})$, σ_{total,K^op}, and $\tau_{K_L^o}$. The absorption cross section in lead was assumed not to vary significantly over the K_L^o spectrum. Three 10 cm. wide scintillators placed side by side at the entrance to the field lens enabled us to improve our knowledge of the pion momentum by a factor of three and of the kaon momentum by approximately a factor of two.

A typical 800 msec Bevatron pulse of 5×10^{11}, 5.6 BeV protons ($\sim$20 % of full beam) produced 12 million beam particles (8 million pions, 2.6 million electrons, 1.4 million muons) incident on the hydrogen target and resulted in about 40 K_L^o's and 700 neutrons entering the decay volume.

A run with the hydrogen target empty produced 1 spark chamber picture of a K decay during an interval in which 97 would have been seen with the target full. The expected number from the end windows and the beam monitor scintillators was 2.

3. THE DETECTORS

A. Basic Configuration

The arrangement of the major components is shown in Fig. 4 and Fig. 5. The spark chambers were arranged around five sides of the cubic decay volume. The center 81 cm x 81 cm of the upstream side was left open for the entering K_L^o mesons which first passed thru the tunnel-like space enclosed by a four-sided, 1.46 m long anti-counter. Each of the five spark chamber units consisted of a front, four-gap aluminum module followed by lead modules. Anti-coincidence scintillators were placed ahead of the lead sections of each chamber. Two banks of trigger counters were placed in the rear (downstream) chamber; one after the first radiation length, and one after the second.

B. The Anti-Tunnel

The anti-tunnel was designed to increase the solid angle subtended by the gamma detection system to about 98 % of 4π in the K center of momentum system. Each of the four counters (T_1 thru T_4) was 1.22 m long, 0.91 m wide, and 5.7 to 8.5 radiation lengths thick. The detailed configuration of material is shown in Fig. 5. The scintillation and Cerenkov light was detected by six 58AVP photomultipliers at the upstream end of each counter. The electron threshold was set close to the one photoelectron level, so that the efficiency was comparable to that of the spark chambers. The final results, however, do not require a knowledge of it, since the $2\pi^o$ events used were required to send all their gammas into the spark chambers, and those $3\pi^o$ events that trigger the chambers and were used for monitoring sent three or more of their gammas into the chambers with essentially unity probability.

C. The Trigger Counters

The two banks of trigger counters placed in the rear spark chamber each contained eleven units placed one above the other. Each unit consisted of a scintillator 0.635 cm x 14 cm x 155 cm and a 3.8 cm thick lucite Cerenkov counter (to prevent np recoil counts) immediately behind the scintillator in the front bank and ahead of it in the rear bank. The lucite slabs of corresponding units in the two banks were brought to one 58AVP phototube (outputs designated C_1 thru C_{11}), while the scintillators were brought to separate two-inch phototubes whose signals were added electronically (outputs designated S_1 thru S_{11}). Six anti-coincidence scintillators (R_1 thr R_6) 0.635 cm x 33 cm x 198 cm placed one above the other between the rear aluminum module and the first lead module made a wall that also served as a cosmic ray anti. To avoid interference with the side chamber support and optics systems the twelve side anti's (A_1 thru A_{12}, three covering each of the four side walls of the decay volume) were mounted inside the four side aluminum chambers.

Placing the trigger counters in the rear rather than the side chambers brought two disadvantages: the spurious trigger rate was high--typically only 6 % of the pictures showed K decays, and the sensitivity to $K_L^o \rightarrow 2\gamma$ was too low to use that as a monitor. The advantages were a relatively high trigger efficiency for both $2\pi^o$ and $3\pi^o$ decays ($\sim$25 %) and the ability to use the same counters for charged decay calibration runs (the charged particles go predominantly forward). Besides, we couldn't figure any way to get the light pipes out of the side chambers without lousing up the optics.

The fast logics block diagram is shown in Fig. 6. The trigger condition for neutral decays was $M_1M_2M_3\bar{L}\,\bar{A}\,\bar{R}\,(SC)_{2-2}$ where $(SC)_{2-2}$ designates any two SC units separated by two or more intermediate units. This separation reduced the spurious trigger rate from single particles crossing from one SC unit to an adjacent one and from groups of low energy gammas coming from the lead filter. Allowing any two such units to provide the trigger also produces one that is free of major kinematic biases.

Placing the tunnel counter signals in anti-coincidence did not greatly reduce the trigger rate, so the information was put on the spark chamber film by having each of the four T counter outputs light one of four gated display lights. The resultant data both provides information on its efficiency and, as mentioned in Part B, makes such information unnecessary, to first order, in calculating the $2\pi^o/3\pi^o$ branching ratio, since the relevant experimental ratio, (number of 4 shower events without T light that pass kinematics)/(number of events with T light + number of events without T light) is independent of the T efficiency to the extent that the numerator comes from $2\pi^o$ events that produce only 4 gammas and hence send none into T.

The SC units also lit display lights placed directly over the ends of the corresponding counters. Events triggered by three or more separated showers then provided a continuous monitor of the SC efficiency.

The trigger condition for charged decays was $M_1 M_2 \overline{M}_3 \overline{L}\ \overline{A}\ R_2 (S)_{2-1}$ where any two of the rear anti's are now required in coincidence and $(S)_{2-1}$ designates any two S counters separated by one or more intermediate units. Because of the R_2 condition, the Cerenkov counter signal was not needed to reduce the spurious trigger rate. Removing this requirement (though leaving the counters in place) was needed for a reliably high efficiency on decay pions and muons, not all of which were fully relativistic.

Relative timing among the S, T, A, R and C counters was done using either gammas from $\pi^- p \rightarrow \pi^o n$ or cosmic rays. Light collection fluctuations in the C counters due to low photostatistics were removed by setting them earlier than the corresponding S and making their discriminator output pulse correspondingly longer. The final timing of the C S T A R group and the $M_1M_2\overline{M}_3\overline{L}$ group was done with K_L^o's by counting spark chamber pictures. All timing curves were required to have flat tops to insure a high and stable efficiency. The resolution times used in the various circuits were necessarily rather broad ($\sim$10-40 ns) due to the differences in the various particle and light collection paths. This caused some accidental triggers, but essentially no accidental events, since the photographs of the K decay events could be identified without ambiguity.

Plateauing was standard, except that since the C counters were operated in the few photoelectron region, the presence of a plateau with voltage does not necessarily guarantee high efficiency. Here efficiency was checked with cosmic rays and with preliminary tests using thinner but otherwise identical slabs.

D. Spark Chambers

The following reasoning led to the choice of lead for the shower spark chamber modules: A limit on the outer size of the cubic array was set by the upper limit on the size of the chambers we were willing to build, and a limit on the inside was set by the required size of the decay volume. These outer and inner limits fixed the chamber thickness, so that the selection of the gap size then set the number of plates. The need to have an adequate number of radiation lengths to convert gammas and fully contain the resultant showers (for spark counting) then sets the number of radiation lengths per plate. On the other hand, efficiency for low energy gammas and maximization of the number of sparks per shower (and thus energy resolution) both require minimizing the ionization energy loss per plate, and also per radiation length. Hence, lead.

The chambers were constructed by laminating two 0.4 mm aluminum sheets to a 0.8 mm lead sheet. Six such plates and one made with only the two aluminum layers were glued to six 3.81 cm wide lucite frames to form one six-gap module. The gap spacing of 8 mm was maintained by gluing 6mm x 6mm x 8mm lucite blocks between the plates at intervals of approximately 20 cm. The faces of these blocks were polished and accurately parallel permitting photography of sparks anywhere in the active volume. The plate edges overhung the lucite frames on all sides and thus were always in air. Besides eliminating edge sparking, this facilitated simple, low-inductance pulser connections. Further construction details will be given elsewhere.

Seven lead modules and one four-gap aluminum module with dimensions of 1.22m x 1.52m formed each side chamber. Eight lead modules and one four-gap aluminum module 1.98m x 1.98m formed the rear chamber. The rear chambers used two separate plates for the right and left halves. Their center edges were glued to a 2.54 cm wide lucite bar that ran from the top to the bottom of each gap. This division point was actually staggered slightly to the right or left of center in adjacent modules.

The pulsers and discharge gaps have been described.[2] The rise times vary somewhat with location, being least on the side opposite the pulsers, but are all about 25 nsec. The fall times were set to be about 35 nsec. in the absence of internal sparks. Shorter rise times would produce serious variations in the peak voltage at different locations within any gap. As it was, the 10kV peak voltage varied by about 800V on the large (rear) chambers. Shorter fall times would begin to reduce the multiple track efficiency. Some of the early data had this failing. A Monte Carlo analysis indicates the value of the result should be relatively insensitive to that variation in efficiency. The analysis of that part of the data, however, has not yet been completed, and it is not included in this report.

Much longer fall times would make spurious sparking probable, but in the range used, this did not happen. (When pulsed at a random time during the beam spill, all 236 gaps would normally have a total of only one or two sparks.) Occasionally sparking developed at the gas tubes, which we had made slightly larger than desirable ($\sim$3mm diameter, $\sim$1-1/2mm would have been better), but it was always curable. The d.c. clearing field was 20V. A pulsed clearing field was also applied after each pulse to remove positive ions, allowing recovery times of about 50 msec. An automatic monitoring system examined the pulse on each double gap and sounded an alarm when the delay time, peak height, or fall time were not within certain preset limits.

Operated in this manner, it was possible to set a 2 spark minimum for gamma showers. (Regenerator studies showed that $2\pi^o$ events had an effective minimum of 4 to 5 sparks. Thus a 2 or 3 spark minimum was of value mainly in rejecting the lower energy gammas coming from $3\pi^o$ background.)

Fig. 4 shows the arrangement of the 10 views on the film. Ten field lenses and 46 front surfaced mirrors were used. The demagnification factor was 138. In addition to the chamber views, the film displayed counter information from the 3 momentum counters (PH, PM, PL), the 4 tunnel counters (T1-T4), the 11 SC units, and a delayed signal (by one Bevatron r.f. cycle) formed from T1 + T2 + T3 + T4 for information on accidentals.

An indication of the energy resolution of the chambers can be seen in Fig. 7 where the total spark count is displayed for 6 shower free decay events and 4 shower regenerator events. The term "equivalent sparks" means that the totals have been increased to allow for oblique traversals of the chamber plates by shower segments and for ionization energy lost in the SC units. The low energy tail on the regenerator events probably comes from $n + Pb \rightarrow 2\pi^o + \ldots$ background. The 6 shower count labeled 1966 shows data taken during the early part of the run when the pulse width was set too short by 5 to 10 nsec resulting in a 10 % shift in the mean number of sparks. No such shifts were seen during the main data run. In addition, the results are insensitive to such shifts since calibration data was available continuously throughout the run.

More detail on the energy resolution and efficiency should come from the $K_L^o \rightarrow \pi^+\pi^-\pi^o$ events that show one or both gammas. Fig. 8 shows our best estimate of the efficiency of the spark chambers for showing showers with two or more sparks in adjacent gaps. The form of the functional dependence is deduced from Monte Carlo shower theory and is then fitted to our observed $3\pi^o \rightarrow 6 : 5 : 4$ shower ratios.

4. THE DATA

A total of 1.8 million spark chamber pictures were taken in the following modes:

(1) Free decay, neutral trigger (45 % of all pictures)

(2) Free decay, charged trigger (18 %)

(3) Regenerator, neutral trigger (32 %)

(a) 12.7 cm thick carbon, 30.5 cm. upstream of rear chamber

(b) 11.8 cm thick beryllium, 30.5 cm upstream of rear chamber

(c) 11.8 cm thick beryllium, 61 cm upstream of rear chamber

(d) 11.8 cm thick beryllium, 86.5 cm upstream of rear chamber

(e) 11.8 cm thick beryllium, separated into 5 slabs spaced uniformly throughout decay volume

(4) Regenerator, charged trigger (5 %)

(a) 11.8 cm thick beryllium, 30.5 cm upstream of rear chamber

(b) 11.8 cm thick beryllium, 61 cm upstream of rear chamber

Beryllium was chosen as the regenerator material primarily because the large cross section of the decay volume combined with the necessary thickness (~ 4 - 5 K_s^o decay lengths) to produce a massive regenerator that would have had a high probability for absorbing large angle gamma rays. Also beryllium has the largest ratio of coherent to incoherent regeneration of any material other than diamond (45 % larger than for graphite of density 1.7, for example). Incoherent regeneration in high A nuclei would have, in this experiment, an angular distribution nearly indistinguishable from that of coherent regeneration, and be useful for all but phase measurements.

However, such regenerators are excluded because of their large gamma absorption.

This data contains pictures of approximately 45,000 neutral K decays, of which approximately 30,000 are without anti-tunnel counts. The following paper will report on an analysis of 19,000 of these taken during the main data run. Analysis of the regenerator and charged decay modes is not yet complete. Following are the number of K decays expected from the preliminary analysis:

Free decay, charged 5000 (all modes) 700 ($\pi^+\pi^-\pi^0$)

Regenerator, neutral

C	- 30.5 cm -	32 (coherent)	117 (incoherent)
Be	- 30.5 cm -	105 "	266 "
Be	- 61 cm -	35 "	89 "
Be	- 86.5 cm -	15 "	38 "
Be	- separated -	16 "	144 "

Scanning has not yet started on the charged regenerator runs.

A potentially serious systematic error can arise if accidental showers are present in the chambers, since this would result in an uncompensated loss of 4 shower - $2\pi^0$ events. To study such possibilities, runs were made in which the chambers were pulsed each time a preset number of beam particles was counted. A preset delay, long compared with the average time between beam particles, made the pulses essentially random ones, but weighted with respect to the average beam intensity in the same way K events would be weighted. R.F. structure considerations did not enter since the chamber clearing time is more than 10 times longer than one R.F. cycle. The results of a 1000 frame run showed:

	Percent of frames	
T 1-4 lights	4.3 %	
T 1-4 delayed lights	4.8 %	
2 spark showers in lead rear chambers	.5 %	2 %
2 spark showers in lead side chambers	.6 %	
≥ 3 spark showers in lead rear chambers	.5 %	
≥ 3 spark showers in lead side chambers	.4 %	
entering charged particle, rear chambers	2.6 %	
entering charged particle, side chambers	.5 %	
n-p recoils	.2 %	
SC lights	.1 %	
PH - PM - PL lights	7.1 %	

Thus the accidental loss of good $2\pi^0$ events is about 4.3 to 4.8 % + 2 % + .1 % $\simeq$ 7 %, since accidental charged particle tracks and n-p recoils do not disqualify events. The low accidental loss due to extra showers is also indicated by the low 7 shower/6 shower ratio. The shower ratios observed are:

7 showers	3 %
6 "	54 %
5 "	36 %

4 showers	6 %
3 "	1 %

The relatively low 4 shower ratio also facilitates the separation of $2\pi^o$ events from the $3\pi^o$ background.

5. CHAMBER AND COUNTER CALIBRATION

Three basic calibration methods are available: one using $3\pi^o$ decays, one using charged decays, and one using regenerated $K_s^o \rightarrow 2\pi^o$ decays. Each is capable of providing (with varying amounts of supplemental calculation) all of the necessary calibration data. Charged decays, especially $\pi^+\pi^-\pi^o$, can provide direct information on the K flux and the chamber and counter efficiencies, but it is necessary to make use of a Monte Carlo program in evaluating the $2\pi^o$ trigger efficiency. Neutral $3\pi^o$ decays can do the same as well as serving as a relative monitor, but require the extensive use of Monte Carlo programs. Regenerator events provide directly the product of the K flux and the overall efficiency. However, corrections must be made for the broader angular distribution of incoherent K's and for gamma absorption within the regenerator. Also the dominant background with regenerator, $n + Be \rightarrow 2\pi^o + \ldots \rightarrow 4$ visible showers, is different from that for free decay, $K_L^o \rightarrow 3\pi^o \rightarrow 4$ visible showers, and presents different subtraction problems. For these reasons, all three methods are being used in this experiment. Table I summarizes their relationship.

TABLE I

	π beam data	$3\pi^0$ decays	all charged decays	$\pi^+\pi^-\pi^0$	regenerator solid	regenerator separated
K spectrum	x			x		
K flux	x	MC	x	MC		
Chamber efficiency		MC		x		
Trigger efficiency		MC		MC		
Spark count calibration		6shower total		x	4shower total	
Angular pointing errors		x		x	x	x

x : data provided directly
MC: data requires Monte Carlo shower theory for evaluation
: product of all three provided subject to corrections mentioned in text

K decay events from the runs in which the regenerator was separated into 5 slabs uniformly spaced throughout the decay volume are almost all from incoherent processes, and hence provide direct information about that important correction. Some information on the relative phase of η_{oo} and η_{+-} may also be available, but will probably be statistically inadequate unless the background (incoherent events in the solid sample passing a θ_k filter) is less than expected.

Acknowledgements

The sustained interest in and support of this experiment by Profs. B. J. Moyer and A. C. Helmholz, particularly at critical junctures, is much appreciated.

We would like to thank David Caldwell who played an important role in early planning and initial decisions.

Roger Chaffee, Neil Evans, and Jerry Nelson gave valuable help in the setup and running of the experiment.

References

1. Precaution taken in operating counters at the high instantaneous rates found in this beam are described in S. I. Parker, W. Oliver, and C. A. Rey, A Photomultiplier Base and Shield System, UCLRL Report.

2. A Compact Low-Inductance Spark Chamber Pulser, S. I. Parker and C. A. Rey, Nuclear Instruments and Methods, 43 (1966) 361. A Triggered Spark Gap for Discharging Spark Chambers, C. A. Rey and S. I. Parker, Nuclear Instruments and Methods, 54 (1967) 314.

Figure Captions

Fig. 1. Beam layout.

Fig. 2. Pion momentum distribution at hydrogen target.

Fig. 3. K_L^o momentum distribution entering decay volume.

Fig. 4. (top) Spark chamber and anti-tunnel array
(bottom) Layout of corresponding spark chamber views on film.

Fig. 5. Side view of spark chamber and counter array.

Fig. 6. Fast electronics block diagram.

Fig. 7. Spark counting results.

Fig. 8. Single photon spark chamber efficiency.

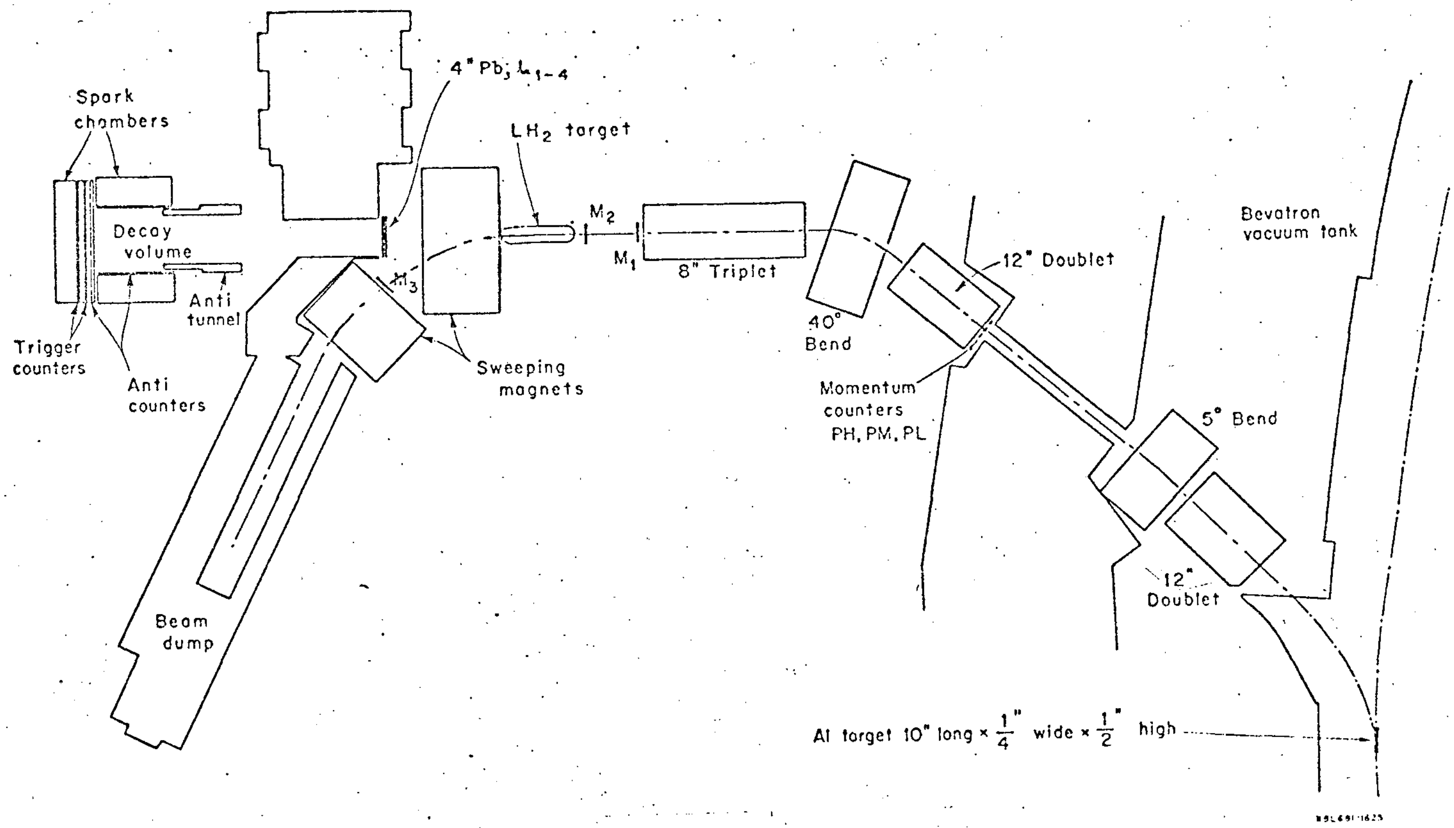
Spark chambers
Decay volume
Anti tunnel
Trigger counters
Anti counters
4" Pb; L_{1-4}
LH_2 target
M_2
M_1
M_3
8" Triplet
40° Bend
12" Doublet
Momentum counters PH, PM, PL
Sweeping magnets
Beam dump
Bevatron vacuum tank
5° Bend
12" Doublet
Al target 10" long × $\frac{1}{4}$" wide × $\frac{1}{2}$" high

Fig. 1

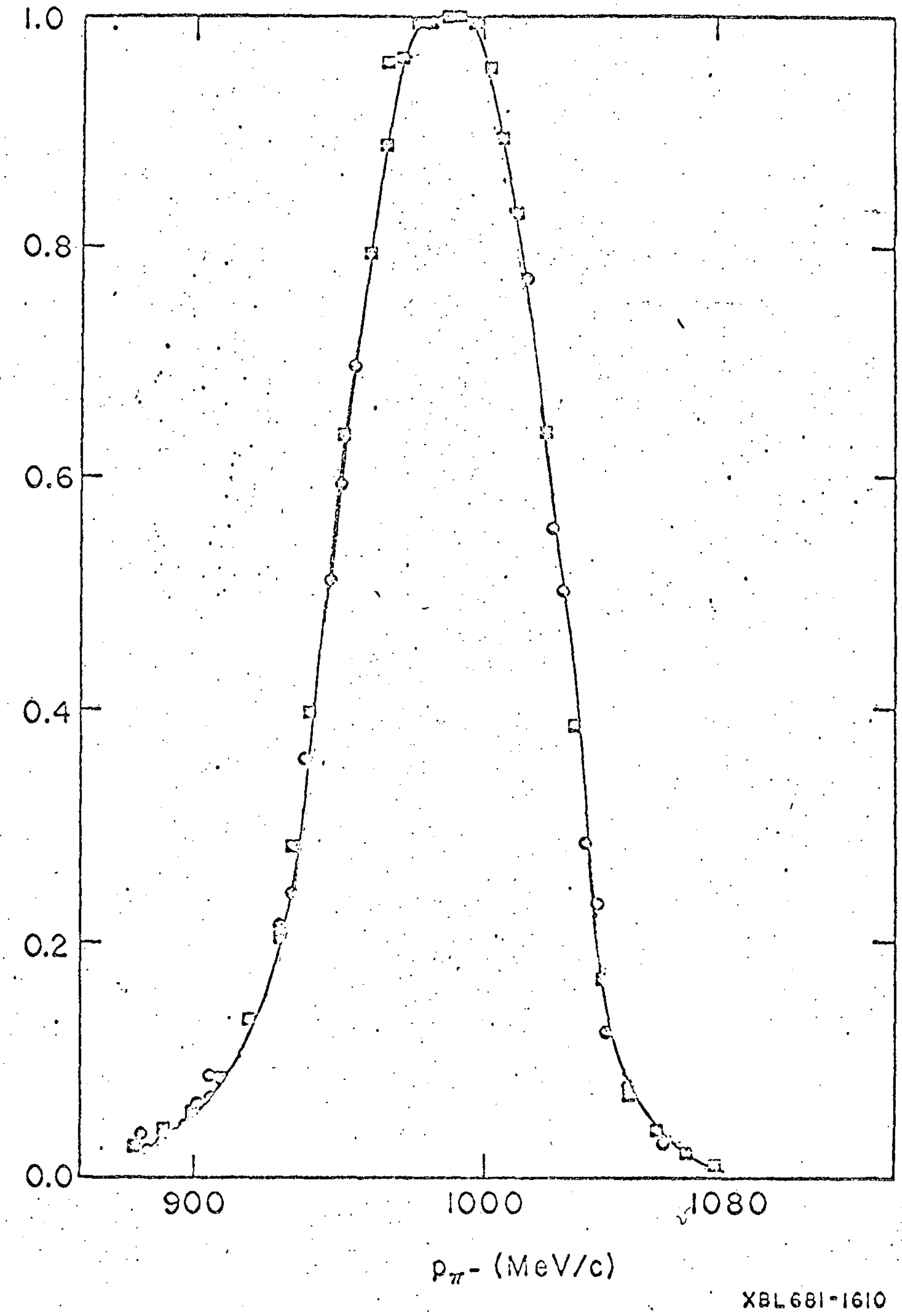

Fig. 2

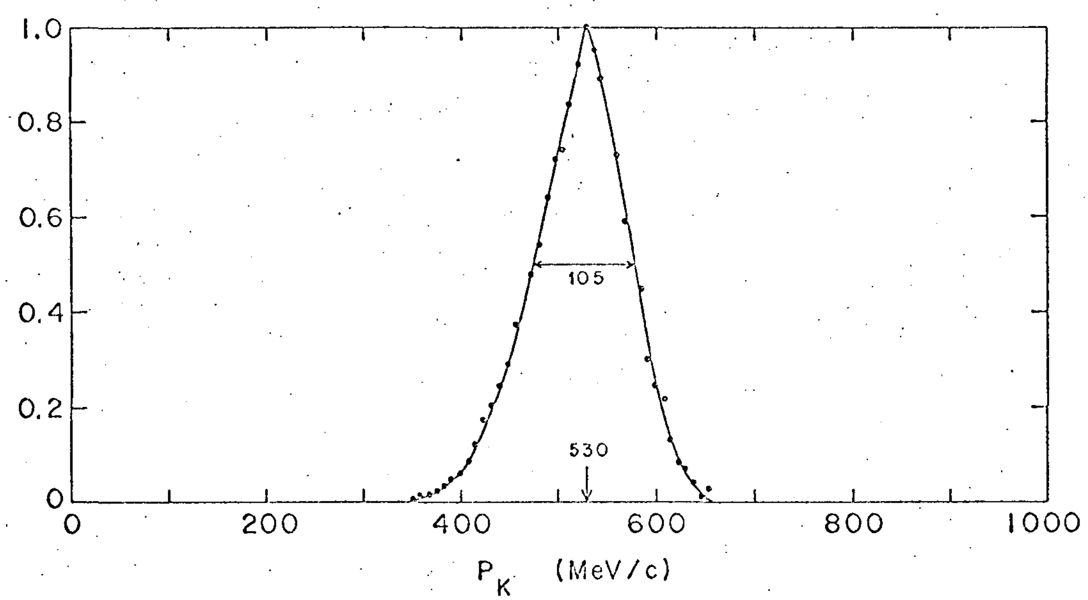

Fig. 3

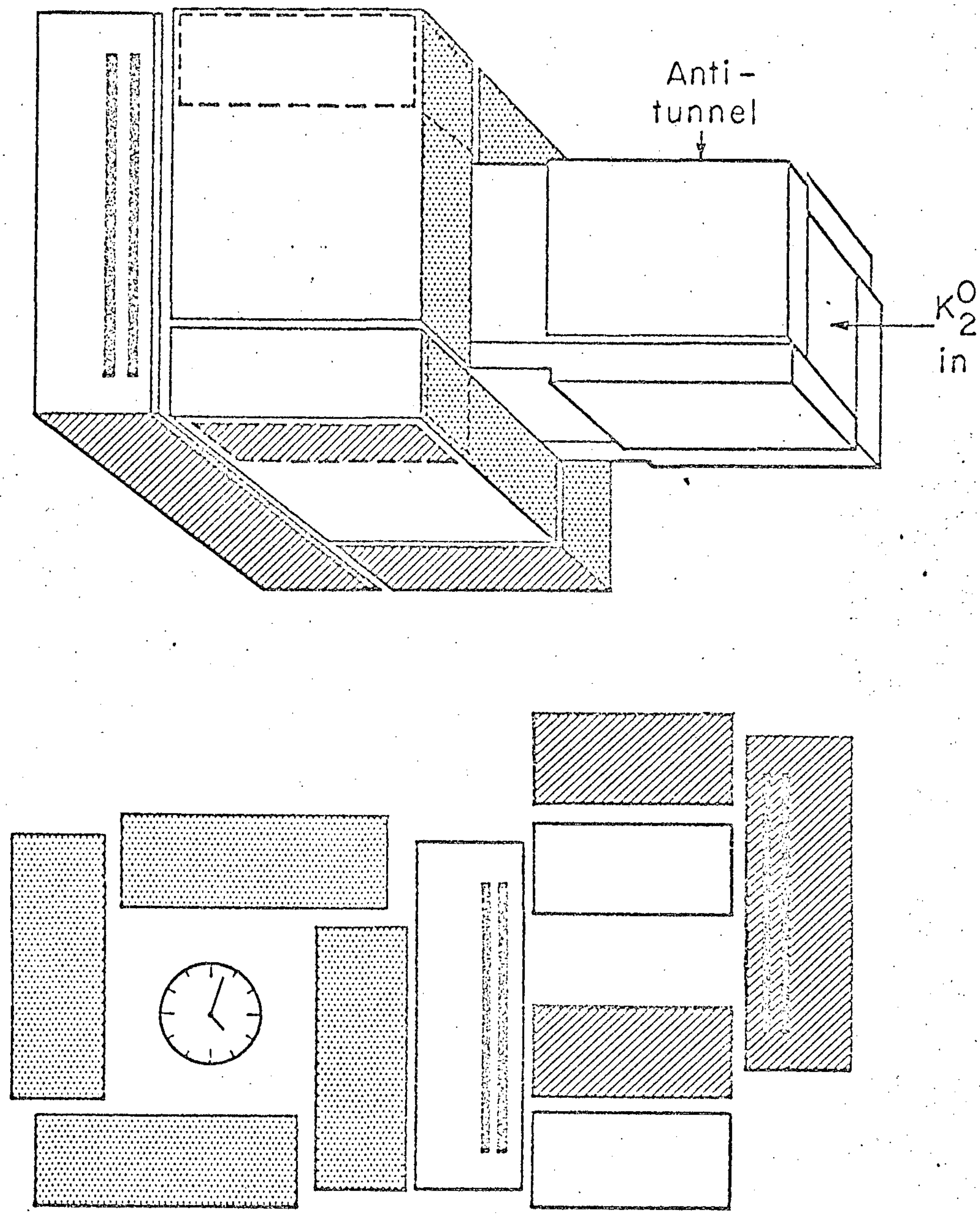

Fig. 4

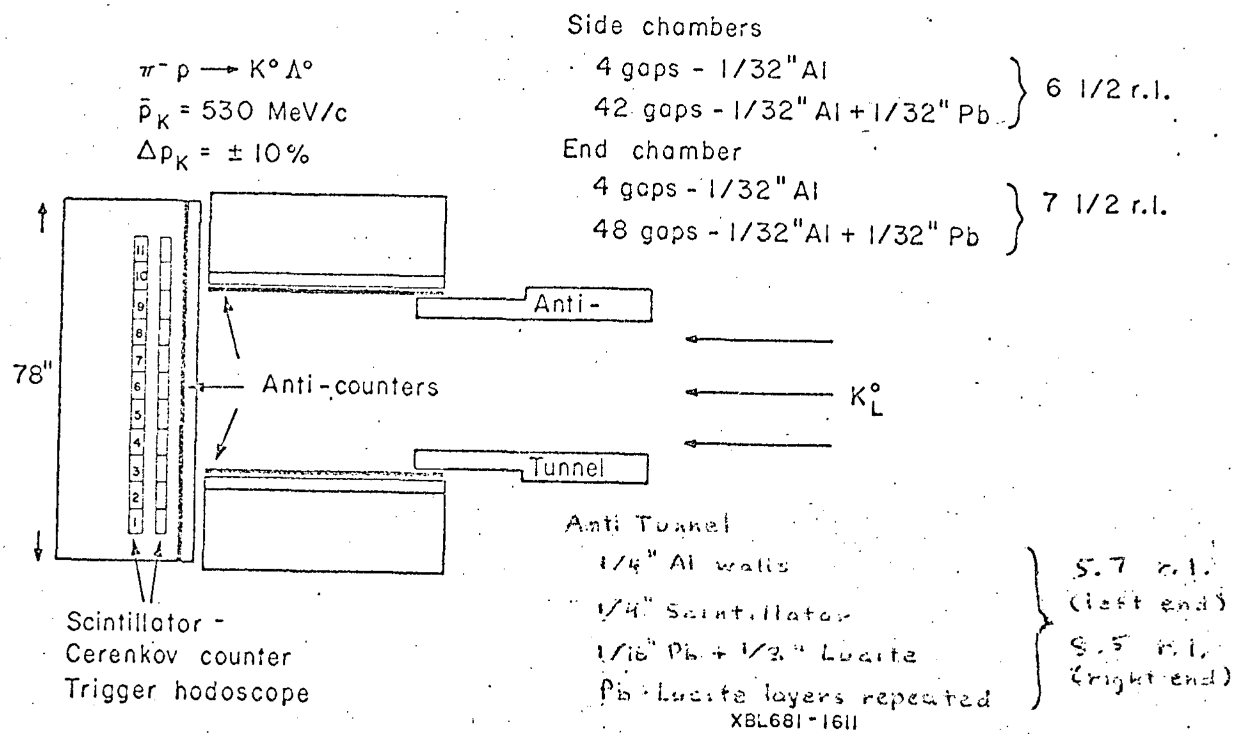
π⁻ p → K° Λ°
p̄K = 530 MeV/c
ΔpK = ± 10%
Side chambers
4 gaps - 1/32" Al
42 gaps - 1/32" Al + 1/32" Pb
6 1/2 r.l.
End chamber
4 gaps - 1/32" Al
48 gaps - 1/32" Al + 1/32" Pb
7 1/2 r.l.
78"
11
10
9
8
7
6
5
4
3
2
1
Anti-counters
Anti-
Tunnel
K°L
Anti Tunnel
1/4" Al walls
1/4" Scintillator
1/16" Pb + 1/2" Lucite
Pb - Lucite layers repeated
5.7 r.l.
(left end)
5.5 r.l.
(right end)
Scintillator -
Cerenkov counter
Trigger hodoscope
XBL681-1611

Fig. 5

To be replaced by simplified diagram as soon as available.

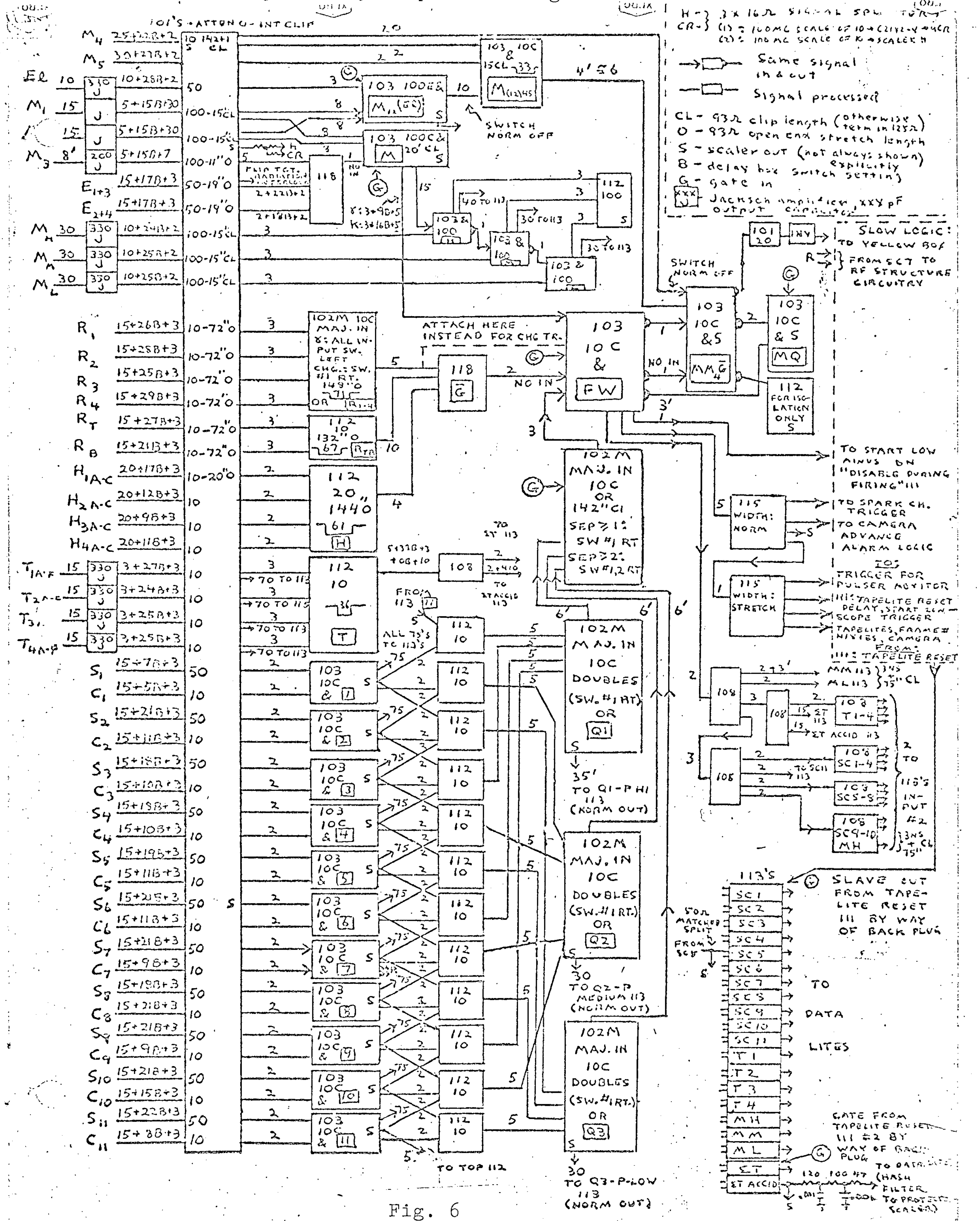

Fig. 6

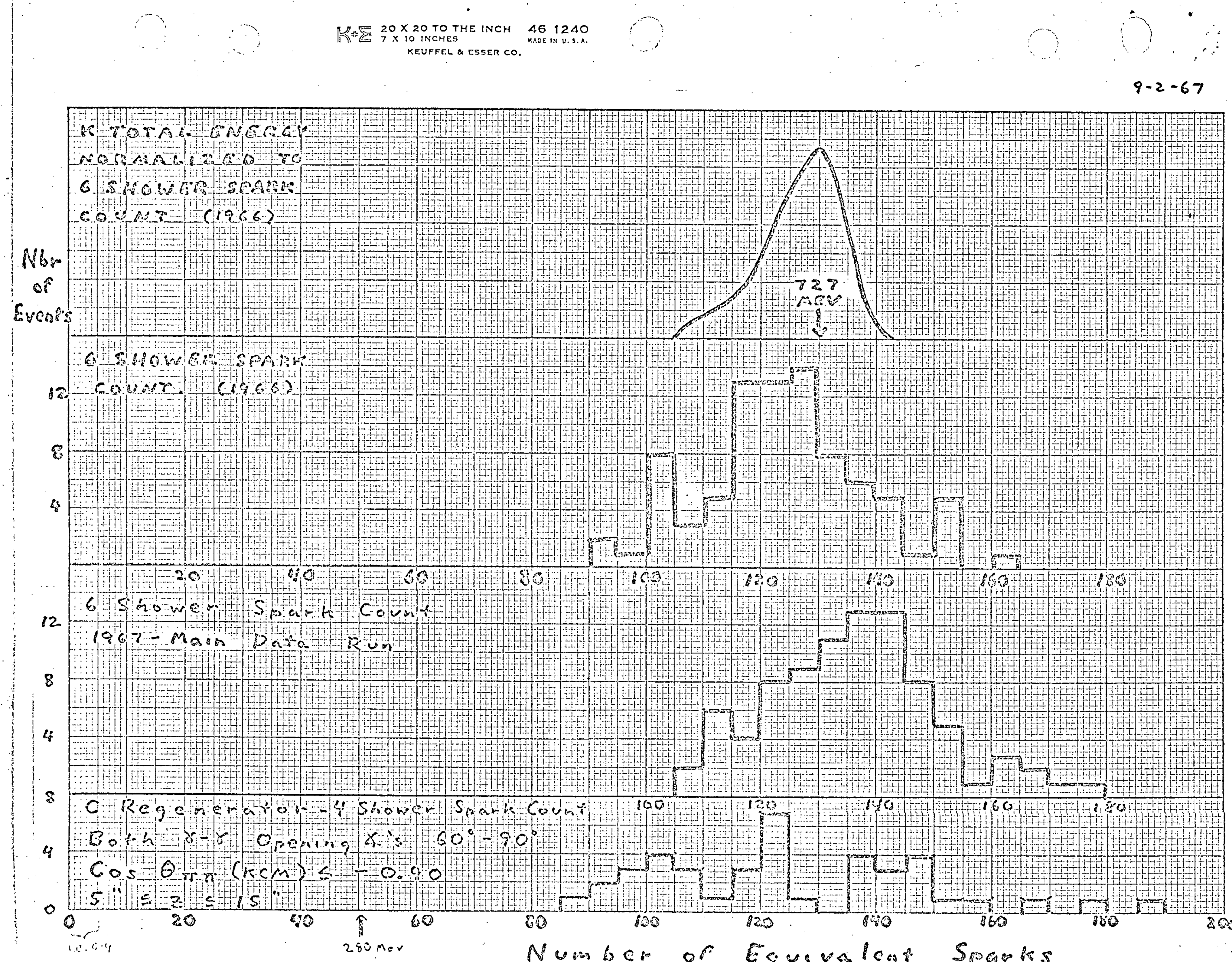
K+E 20 X 20 TO THE INCH 7 X 10 INCHES KEUFFEL & ESSER CO. 46 1240 MADE IN U.S.A.
9-2-67
K TOTAL ENERGY NORMALIZED TO 6 SHOWER SPARK COUNT (1966)
727 MeV
6 SHOWER SPARK COUNT. (1966)
6 Shower Spark Count 1967 - Main Data Run
C Regenerator - 4 Shower Spark Count
Both γ-γ Opening ∠'s 60°-90°
Cos θππ (KCM) ≤ -0.90
5" ≤ z ≤ 15"
Nbr of Events
0
4
8
12
20
40
60
80
100
120
140
160
180
200
280 MeV
Number of Equivalent Sparks

Fig. 7

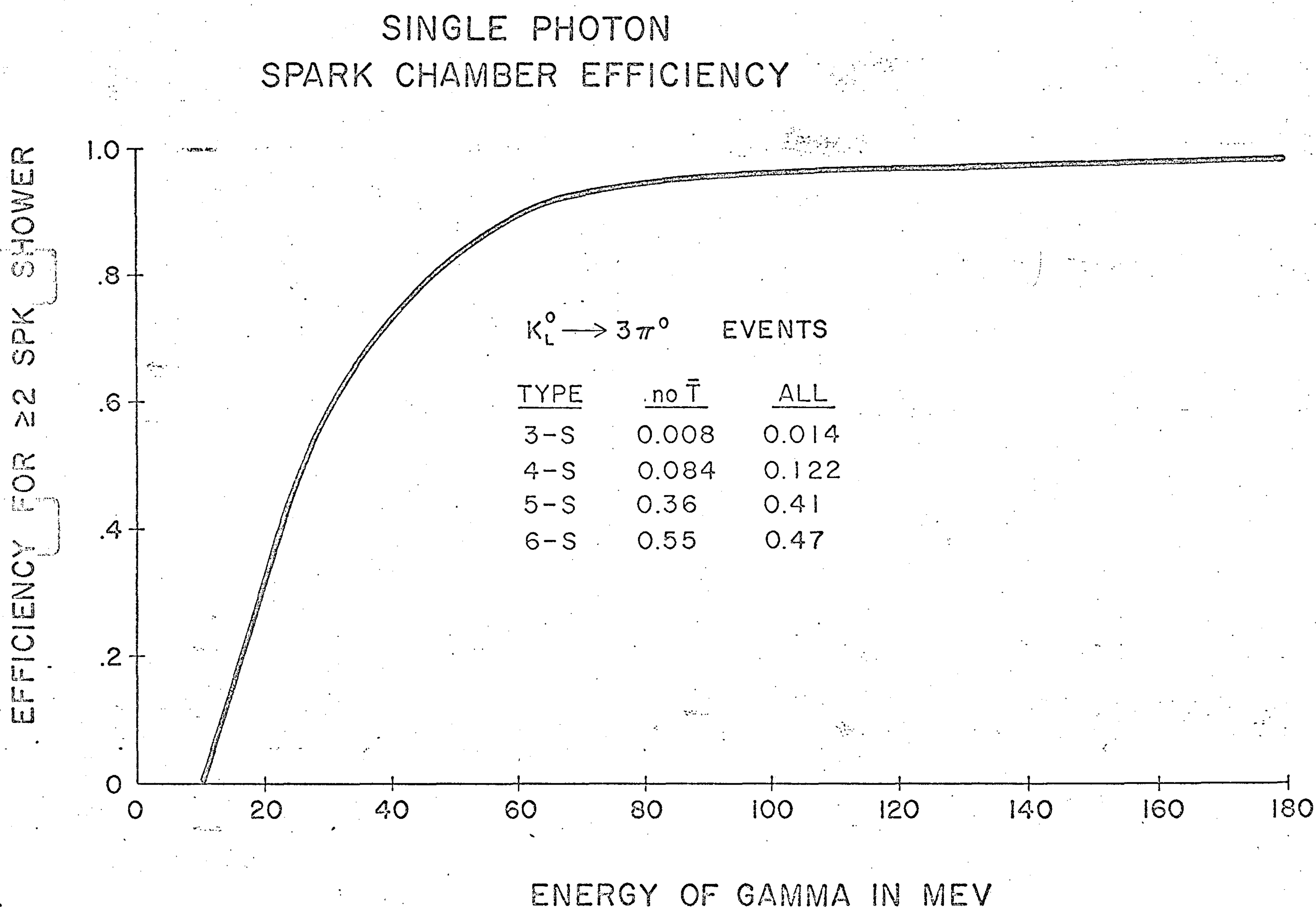
SINGLE PHOTON
SPARK CHAMBER EFFICIENCY
EFFICIENCY FOR ≥2 SPK SHOWER
ENERGY OF GAMMA IN MEV
1.0
.8
.6
.4
.2
0
0
20
40
60
80
100
120
140
160
180
$K_L^0 \longrightarrow 3\pi^0$ EVENTS
TYPE no $\bar{T}$ ALL
3-S 0.008 0.014
4-S 0.084 0.122
5-S 0.36 0.41
6-S 0.55 0.47

Fig. 8